Nanosphere Lithography: Surface Plasmon Resonance Spectrum of a Periodic Array of Silver Nanoparticles by Ultraviolet−Visible Extinction Spectroscopy and Electrodynamic Modeling

Traci R. Jensen, George C. Schatz,* and Richard P. Van Duyne*

Department of Chemistry, Northwestern University, Evanston, Illinois 60208-3113

Received: November 11, 1998; In Final Form: February 5, 1999

In this paper we measure the optical extinction spectrum of a periodic array of silver nanoparticles fabricated by nanosphere lithography (NSL) and present detailed comparisons of the results with predictions of electrodynamic theory. The silver nanoparticles are small (∼100 nm) compared to the wavelength of light but too large to have their optical properties described adequately with a simple electrostatic model. We make use of the discrete dipole approximation (DDA), which is a coupled finite element method. With the DDA one can calculate the extinction of light as a function of wavelength for particles of arbitrary size and shape. We show that NSL-fabricated Ag nanoparticles can be modeled without adjustable parameters as truncated tetrahedrons, taking their size and shape parameters directly from atomic force microscopy (AFM) measurements and using literature values of the bulk dielectric constants of silver. These AFM measurements are presented as part of this paper, and the resulting theoretical line shapes and peak widths based on the AFM-derived parameters are in good agreement with measured extinction spectra. The peak width measured as the full width at half-maximum (fwhm) is approximately 100 nm, or 0.35 eV, which corresponds to an electron−hole pair lifetime of 2 fs. The combined effects of particle−particle and particle−substrate interactions red-shift the surface plasmon resonance by only about 10 nm versus a single isolated particle. By use of AFM-derived parameters that have been corrected for tip-broadening and by inclusion of an estimate for the effects of particle−particle and particle−substrate interaction, the discrepancy between the theoretical and experimental extinction peak maxima is approximately 25 nm, which is significantly smaller than the plasmon width. This residual difference between theory and experiment is due to shortcomings of the truncated tetrahedron geometry in describing the actual shape of the particles, errors in the literature values of the bulk dielectric constants, and experimental uncertainty due to slight heterogeneities in nanoparticle structure.

I. Introduction

There is currently intense interest in examining the optical properties of nanosized metal particles, which differ greatly from those of the bulk material.[1−6] When metal nanoparticles are excited by light, they exhibit collective oscillations of their conduction electrons known as surface plasmons. The resonance energy of the surface plasmon is strongly dependent on the details of the size and shape of the nanoparticle, the dielectric properties of the metal from which the nanoparticle is composed, and the dielectric properties of the local environment in which the nanoparticles are embedded. Surface plasmon resonance spectra have been measured from metal island films,[7−9] colloids,[10−17] and lithographically prepared metal particles.[18−21] Several excellent reviews discuss both the experimental and theoretical aspects of nanoparticle optics.[22−24]

Attempts have been made to model the surface plasmon resonance spectra of nanoparticles using various implementations of electrodynamic theory. One example is Mie theory, which is an exact analytical solution to Maxwell's equations that applies only to isolated spheres.[24,25] Mie theory can be used to quantitatively model the extinction spectra of colloids, and the match between theory and experiment is excellent as long as the colloids are spherical in shape, dilute, and relatively monodisperse.[26,14] To obtain an analytical solution for simple shapes other than spheres, an electrostatic approximation must be used. This is the long-wavelength limit solution of Maxwell's equations. Ellipsoidal nanoparticles that are small compared to the wavelength of light have been modeled using an electrostatic approximation with certain corrections introduced to account for size effects.[19,21] Effective medium approximations such as the Maxwell−Garnett and Bruggeman theories have been used to model the optical extinction spectra of ellipsoids when interparticle interactions cannot be neglected.[7,13,27,28] Both theories rely on the assumption that the particle size is small compared to the wavelength of light.

To date, only these simple theories based on the small-particle assumption have been used to model the optical properties of nonspherical nanoparticles. An exception is the numerical approximation known as the **T**-matrix scattering treatment, which has been applied to spheroids and other axiosymmetric particles.[29−31] However, **T**-matrix methods are only available for certain particle shapes, and it is difficult to achieve convergence of the results for larger-sized particles. Another problem in obtaining a quantitative match between theory and experiment is that often the nanoparticles under study either are not homogeneous in shape and size or are simply not well characterized. Often, the shape and/or size of the nanoparticle is used as fitting parameters in the calculation in order to achieve the best fit to experimental results.

* To whom correspondence should be addressed. E-mail: schatz@chem.nwu.edu, vanduyne@chem.nwu.edu.

10.1021/jp984406y CCC: $18.00
Published on Web 03/13/1999

Recent advances in nanolithographic technology have made it possible to prepare nearly homogeneous arrays of nanoparticles with tunable sizes and shapes.[32,33] These experimental advances provide challenging problems for electrodynamics theory. To solve for optical properties such as the scattering and absorption cross sections of nanoparticles of arbitrary shape, one must turn to numerical solutions, which until recently have only been performed for particles of limited shapes and sizes because of the complexity and computational cost of the problem.

Advances in electrodynamics methods have made it possible to overcome the difficulties associated with evaluating the optical response for particles of arbitrary shape.[34,35] A method known as the discrete dipole approximation (DDA) is well-suited for this application.[36−38] The method involves replacing the particle of interest by a cubic array of dipoles, each of which has an oscillating polarization that is determined by the local dielectric constant, the incoming electromagnetic field, and interaction with the other dipoles. The response of the collection of dipoles to an applied field can then be described by self-consistently determining the induced dipole in each element. Using this information, one can then solve for the scattering and absorption cross sections of the particle. In the limit of an infinite number of dipole elements, the DDA provides a nearly exact solution to Maxwell's equations.

In this paper we show that when the DDA is used, it is possible to obtain excellent agreement between the experimentally measured extinction spectrum of tetrahedral-shaped nanosized silver particles and the results of electrodynamic theory. The structure of the Ag nanoparticles, which we have measured with AFM, is directly input along with the known wavelength-dependent dielectric constants of bulk silver into the DDA calculation. Therefore, no adjustable parameters have been used in order to obtain the best fit between theory and experiment.

The remainder of this manuscript will progress as follows. In section II we will discuss the experimental details involved in fabricating the array of tetrahedral silver particles and measuring their structural and optical properties. In section III we will give a brief description of the DDA method and details of the calculations. In section IV we will present the experimental results and show the relevant calculations for modeling the experimental extinction spectrum, and in section V we will summarize our conclusions.

II. Experiment

A. Preparation of Periodic Particle Arrays. Single-layer periodic particle arrays were prepared by nanosphere lithography.[32] A suspension of 400 ± 7 nm polystyrene nanospheres (Interfacial Dynamics Corporation, Portland, OR) was drop-coated onto a mica substrate approximately 1 cm^2 in area and 50 μm thick. The nanospheres self-assembled to form a hexagonal close-packed monolayer that acts as a material deposition mask. Ruby red muscovite was purchased from Asheville-Schoonmaker Mica Co. (Newport News, VA). The nanospheres were received as a suspension in water and were further diluted in a 1:1 ratio with a solution of the surfactant Triton X-100 and methanol (1:400 by volume) in order to allow for better packing over large areas of the substrate. Samples were then mounted into the chamber of a Consolidated Vacuum Corporation vapor deposition system. Approximately 50 nm of Ag (99.99%, purchased from D. F. Goldsmith, Evanston, IL) was deposited at a rate of 0.2 nm/s as measured by a Leybold Inficon XTM/2 deposition monitor quartz crystal microbalance (East Syracuse, NY). After Ag deposition, the nanosphere mask was removed by sonicating the samples in CH_2Cl_2 for 2 min, leaving behind a hexagonal array of truncated tetrahedral-shaped silver particles.

B. Ultraviolet−Visible Extinction Spectroscopy. Transmission mode extinction measurements were performed on a Beckman DU-7 UV−vis spectrophotometer. Optical extinction is the sum of scattering and absorption. Extinction is defined as $-\log(I_t/I_o)$, where I_o and I_t are the incident and transmitted light intensities, respectively. Samples were placed in a thin cell cuvette, and dry nitrogen was flowed through the cell. An initial extinction spectrum was measured representing the surface plasmon resonance (SPR) of the nanoparticle array in ambient conditions, and then measurements were taken repeatedly as the nitrogen flowed over the sample until the position of the SPR stabilized and represented that of the nanoparticle array under dry nitrogen conditions. The position of the SPR is quite sensitive to the external dielectric environment of the nanoparticles. This issue will be thoroughly addressed in another paper.[39] All extinction measurements were referenced to the background spectrum of a blank mica substrate of the same thickness as the sample. The rectangular sample area probed by the spectrometer was approximately 2 mm × 4 mm, and the probe beam was unpolarized.

C. Atomic Force Microscopy (AFM) Measurements. AFM images were collected under ambient conditions on a Digital Instruments Nanoscope III microscope. Etched Si nanoprobe tips (Digital Instruments, Santa Barbara, CA) were used. These tips have spring constants of approximately 0.15 N m^{-1} and are conical in shape with a cone angle of 20° and an effective radius of curvature at the tip of 10 nm. The AFM images presented here represent raw, unfiltered data collected in constant-force mode.

III. Theory: Discrete Dipole Approximation (DDA)

In the DDA method, the particle of interest, which can be of any arbitrary shape, is divided into a cubic array of N-point dipoles with polarizabilities denoted as $\boldsymbol{\alpha}_i$ and centers at position $\mathbf{r}_i$. The interaction of each dipole with a local electric field $\mathbf{E}_{loc}$ will induce a polarization given by (omitting frequency factors $e^{i\omega t}$):

$$\mathbf{P}_i = \boldsymbol{\alpha}_i \cdot \mathbf{E}_{loc}(\mathbf{r}_i) \tag{1}$$

$\mathbf{E}_{loc}$, for isolated particles, is the sum of the incident field and the field $\mathbf{E}_{self}$ from all other dipoles in the particle,

$$\begin{aligned}\mathbf{E}_{loc}(\mathbf{r}_i) &= \mathbf{E}_{loc,i} = \mathbf{E}_{inc,i} + \mathbf{E}_{self,i} \\ &= \mathbf{E}_0 \exp(i\mathbf{k}\cdot\mathbf{r}_i) - \sum_{j\neq i} \mathbf{A}_{ij}\cdot\mathbf{P}_j\end{aligned} \tag{2}$$

$\mathbf{E}_0$ and $\mathbf{k}$ are the amplitude and wave vector of the incident wave, respectively. The interaction matrix $\mathbf{A}$ has the form

$$\mathbf{A}_{ij}\cdot\mathbf{P}_j = \frac{\exp(ikr_{ij})}{r_{ij}^3}\left\{k^2\mathbf{r}_{ij}\times(\mathbf{r}_{ij}\times\mathbf{P}_j) + \frac{(1-ikr_{ij})}{r_{ij}^2}\times [r_{ij}^2\mathbf{P}_j - 3\mathbf{r}_{ij}(\mathbf{r}_{ij}\cdot\mathbf{P}_j)]\right\} \qquad (j\neq i) \tag{3}$$

where $k = \omega/c$.

If the system of interest consists of more than one particle on top of a flat substrate, then $\mathbf{E}_{loc,i}$ will have additional contributions. These will include a field $\mathbf{E}_{ref,i}$ due to reflection of the incident field from the substrate, a field $\mathbf{E}_{others,i}$ due to

fields from dipoles on other particles (the interparticle interaction), and a field $\mathbf{E}_{subs,i}$, arising from the reflection of dipole radiation due to all the particles from the substrate (the substrate effect). Therefore, the local field in this more general case can be expressed as

$$\mathbf{E}_{loc,i} = \mathbf{E}_{inc,i} + \mathbf{E}_{ref,i} + \mathbf{E}_{self,i} + \mathbf{E}_{others,i} + \mathbf{E}_{subs,i} \quad (4)$$

where

$$\mathbf{E}_{ref,i} = F_{||,\perp}\mathbf{E}_0 \exp(\mathbf{k}'\cdot\mathbf{r}_i)$$
$$\mathbf{E}_{others,i} = \sum_{j'}{}'\mathbf{A}_{ij}\cdot\mathbf{P}_j$$
$$\mathbf{E}_{subs,i} = -\sum_{j}\mathbf{A}_{ij}\cdot\mathbf{P}''_j \quad (5)$$

The reflection term, $\mathbf{E}_{ref,i}$, includes the Fresnel coefficient F for either parallel or perpendicular polarization. The wave vector of the field reflected from the substrate is denoted $\mathbf{k}'$. The interparticle interaction term, $\mathbf{E}_{others,i}$, includes the sum over all dipoles except those on the same particle as i, while the substrate term, $\mathbf{E}_{subs,i}$, includes contributions from all dipoles including i. The interaction matrix A_{ij} is given by eq 3 for both these terms. The polarization $\mathbf{P}''_j$ appearing in the substrate term is obtained from $\mathbf{P}_j$ using the image model formulas:

$$\mathbf{P}''_{||j} = -\frac{\epsilon_{subs} - 1}{\epsilon_{subs} + 1}\mathbf{P}_{||j}$$
$$\mathbf{P}''_{\perp j} = \frac{\epsilon_{subs} - 1}{\epsilon_{subs} + 1}\mathbf{P}_{\perp j} \quad (6)$$

where || and $\perp$ refer to the parallel and perpendicular components relative to the surface of the substrate.

Substituting eqs 2−5 into eq 1 and rearranging terms, we generate an equation of the form

$$\mathbf{A}'\cdot\mathbf{P} = \mathbf{E} \quad (7)$$

where $\mathbf{A}'$ is a matrix that is built out of the matrix $\mathbf{A}$ from eq 3. For a system with N total dipoles, $\mathbf{E}$ and $\mathbf{P}$ are $3N$-dimensional vectors, and $\mathbf{A}'$ is a $3N \times 3N$ matrix. Solving this set of $3N$ complex linear equations allows the polarization vector $\mathbf{P}$ to be obtained and consequently the optical properties such as the extinction cross section to be calculated.

To solve this system of $3N$ complex linear equations, we use an adaptation of an approach developed by Draine and Flatau. They have developed a program[40] that utilizes fast Fourier transform methods to perform the sum over dipole fields in eqs 2, 4, and 5 and complex conjugate gradient techniques to solve eq 6. The polarizability of each dipole is assumed to follow the lattice dispersion relation (LDR) proposed by Draine and Goodman.[38] The LDR ensures that in the limit of an infinite number of dipoles the correct Maxwell solution will be obtained.

IV. Results and Discussion

Figure 1A shows a large-scale (15 μm × 15 μm) AFM image of a Ag periodic particle array with typical defect sites labeled. A defect site such as that labeled 1 results from a missing nanosphere in the deposition mask, while a site such as that labeled 2 represents an example of a slip dislocation in the nanosphere packing. Figure 1B shows a more detailed (1 μm × 1 μm) view of a single hexagon of nanoparticles. It is evident that, in this planar view, the nanoparticles are approximately triangular in cross section. The in-plane width of a nanoparticle, "a", will therefore refer to the perpendicular bisector of the base of the nanoparticle. The in-plane width and out-of-plane height of the particles in the array were directly measured using AFM and found to be "a" = 120 ± 8 nm and "b" = 46 ± 2 nm, respectively. The tip-to-tip distance, d_{tt}, between particles in the array was measured to be 114 ± 9 nm. The lateral dimensions of the particle as reported have not been corrected for the broadening caused by tip convolution. This point will be discussed in detail later in this section.

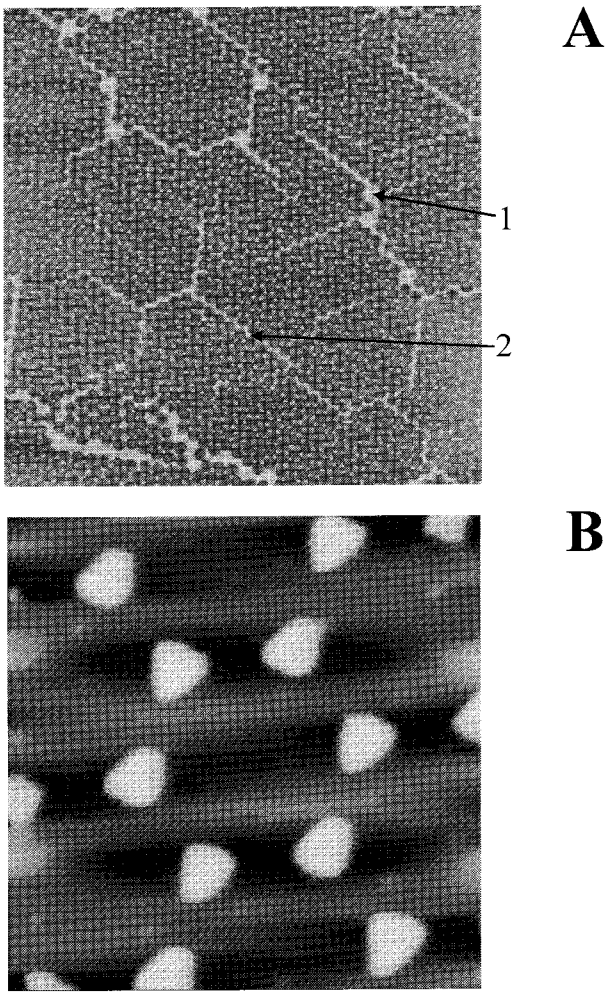

Figure 1. AFM micrographs showing. (A) 15 μm × 15 μm area nanoparticle array with typical defect areas shown. Arrow labeled 1 represents site of missing nanosphere in deposition mask. Arrow labeled 2 shows example of slip dislocation in nanosphere mask. (B) 1 μm × 1 μm area hexagonal array of particles.

The measured UV−vis extinction spectrum of the nanoparticle array is shown in Figure 2. This represents the macroscopic, far-field result measured with unpolarized light. The peak extinction wavelength is at 586 nm, and the width of the surface plasmon resonance measured as fwhm is 100 nm, or 0.35 eV. This measurement was performed several times, and the range of values obtained was 578−590 nm. The oscillatory noise seen in the data is lowest in frequency at long wavelengths and becomes less significant as the thickness of the mica substrate is increased (data not shown). Therefore, we attribute this phenomenon to interference of the probe beam between the front and back faces of the mica substrate. To model the surface plasmon resonance spectrum using DDA theory, we must know not only the nanoparticle dimensions "a" and "b" but also their detailed shape.

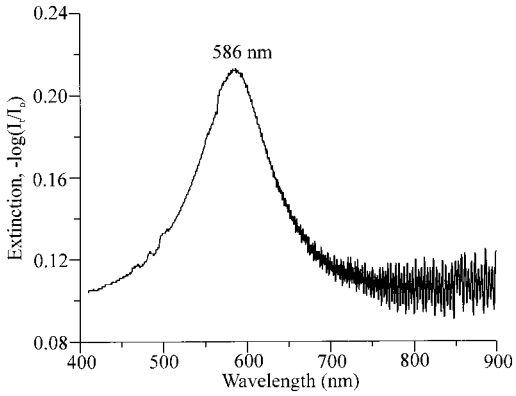

Figure 2. Macroscopic, far-field UV−vis extinction spectrum of nanoparticle array shown in Figure 1. $\lambda_{max} = 586$ nm.

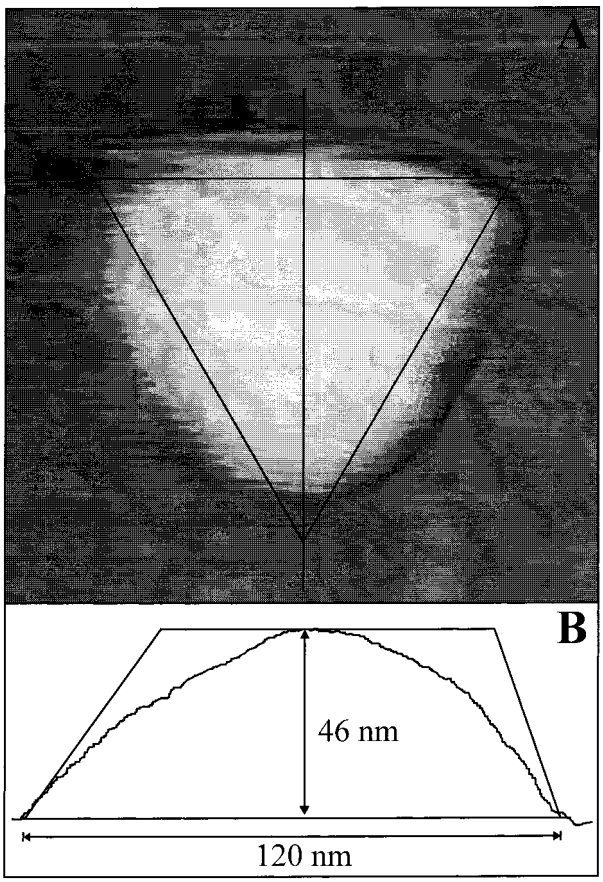

Figure 3. (A) AFM micrograph showing 200 nm × 200 nm image of a single particle. Equilateral triangle having a perpendicular bisector of 120 nm is superimposed. (B) Line scan of particle taken along perpendicular bisector drawn in part A. Cross section of ideal truncated tetrahedron shape is superimposed on the line scan.

Figure 3A shows a higher resolution (200 nm × 200 nm) AFM image of a single nanoparticle. An equilateral triangle having a perpendicular bisector of 120 nm is superimposed on the particle. Although the cross-sectional shape is roughly triangular, there is some deviation from triangular shape at the tips of the nanoparticle. We have found from previous work that, for silver, deviations from a triangular in-plane shape are a systematic function of the nanosphere diameter used in the deposition mask. These deviations begin when the nanosphere diameter is less than about 500 nm.[33] Figure 3B shows the line scan taken along the perpendicular bisector of the particle. The simplest ideal geometric shape that approximates the actual

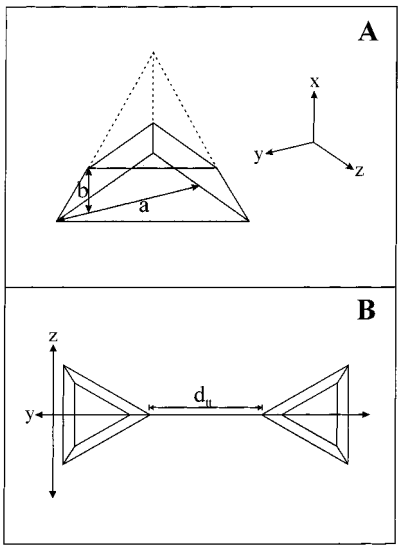

Figure 4. (A) Schematic of truncated tetrahedron. (B) Schematic of two truncated tetrahedra with axes indicated.

shape of the particle is that of a truncated tetrahedron. This shape is defined by "slicing off" one tip from a regular tetrahedron such that the plane of the slice is parallel to the plane associated with the opposite face of the tetrahedron, which we refer to as the base. The length of the perpendicular bisector of the base is the width of the particle, denoted as "*a*". The distance between the two parallel planes is denoted as "*b*" and is in effect the height of the particle (Figure 4A). The ideal cross-sectional line scan along the perpendicular bisector of a truncated tetrahedron with "*a*" = 120 nm and "*b*" = 46 nm is superimposed on the measured line scan of the particle in Figure 3B. Once again, we see that there is significant rounding of the corners of the particle. However, the truncated tetrahedron model has the advantage of being a simple geometry to use in the DDA calculation and is a good first approximation to the actual shape of the particle.

Bulk dielectric constants for silver, ϵ_{Ag}, are the last parameter that must be input to the DDA calculation. We use values from Palik[41] unless otherwise stated. However, we will examine the effect of the choice of dielectric constant on the calculated extinction spectrum for three different sets of dielectric constants from the literature: those of (1) Palik, (2) Hagemann, Gudat, and Kunz,[42] and (3) Johnson and Christy.[43]

The direction of incident light in the calculations is taken to be perpendicular to both the plane of the slice of the tetrahedron and the plane that coincides with the substrate, as it is in the experiment. This is labeled arbitrarily as the *x*-axis, and the *y*-axis is chosen to be along the axis of the perpendicular bisector of the base (see Figure 4A). Some calculations were done with two truncated tetrahedra arranged such that their bases lie in the same plane, and the perpendicular bisectors of each base lie on the *y*-axis with tips pointed toward each other. The distance between the particles is measured from tip to tip and is given the designation d_{tt} (see Figure 4B). Calculations have been done using *y*-polarized incident light unless otherwise stated.

All results will be presented as extinction efficiencies, which are the ratio of the calculated extinction cross sections to the cross-sectional area of the sphere whose volume is equal to that of the truncated tetrahedron.

We first examine the convergence properties of the DDA calculation for a single isolated truncated tetrahedron. Figure 5 shows the calculated extinction spectrum using 544, 2498, 6854,

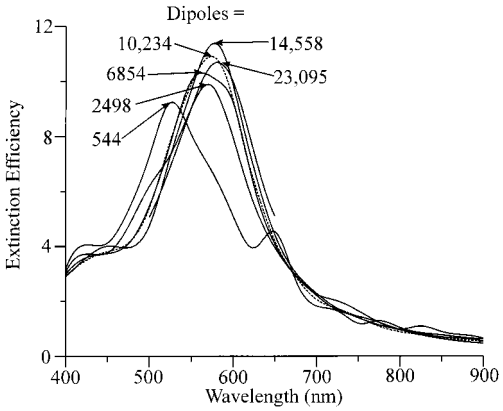

Figure 5. Convergence properties of the extinction spectrum of a truncated tetrahedron having a width "*a*" = 120 nm and height "*b*" = 46 nm. Results calculated using 544, 2498, 6854, 10 234, 14 558, and 23 095 dipoles are shown. Dielectric constants of Palik are used, and the polarization direction is chosen to be along the *y*-axis.

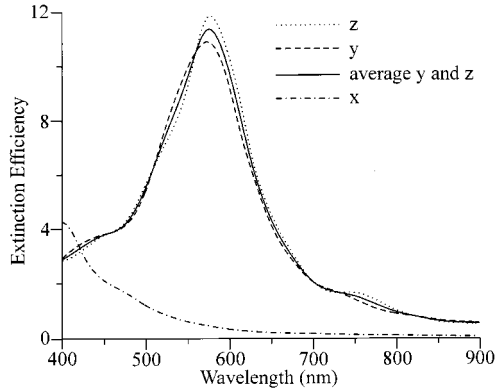

Figure 6. Polarization dependence of the extinction spectrum for a truncated tetrahedron calculated using 10 234 dipoles. Polarizations along the *x*-, *y*-, and *z*-axes are shown, as well as the averaged result of *y*- and *z*-polarizations, which best represents experimental conditions. λ_{max}(*z*-pol) = 578 nm, λ_{max}(*y*-pol) = 574 nm, λ_{max}(*x*-pol) = 399 nm, λ_{max}(*yz*-pol) = 577 nm.

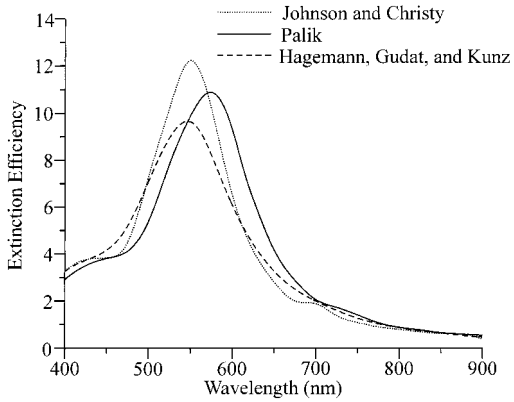

Figure 7. Effect of choice of dielectric constant for silver on the extinction spectrum of truncated tetrahedron. Calculation uses 10 234 dipoles and assumes *y*-polarized incident radiation. Results are shown calculated using bulk ϵ_{Ag} of Palik (λ_{max} = 574 nm), Johnson and Christy (λ_{max} = 550 nm), and Hagemann, Gudat, and Kunz (λ_{max} = 548 nm).

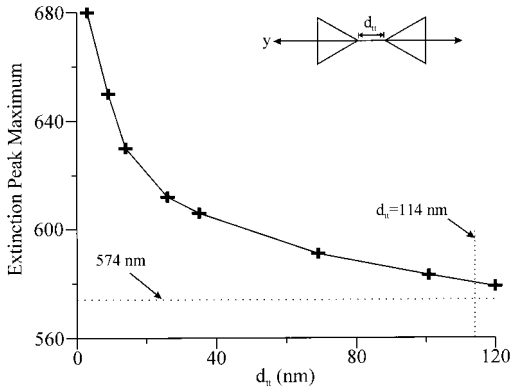

Figure 8. Effect of particle−particle interaction on the extinction spectrum of two truncated tetrahedra. The extinction peak maximum is plotted as a function of d_{tt}. Results are calculated using 10 234 dipoles in each particle, dielectric constants from Palik, and polarization along the *y*-axis. The solid lines are a guide for the eye.

10 234, 14 558, and 23 095 dipoles. We find that the result using about 10 000 dipoles represents a satisfactory balance between sufficient convergence of the calculation and practical time constraints involved in the calculation. This corresponds to the condition that each cubic element composing the target be approximately 3 nm on a side, or 27 nm^3.

Figure 6 shows the electric field polarization dependence of the calculated extinction spectrum of a single isolated truncated tetrahedron. The SPR excited by *y*-polarized light peaks at 574 nm, while *z*-polarized light causes a SPR peak at 578 nm and an approximately 7% decrease in the value of the extinction efficiency at the peak wavelength. Overall, there is only a small difference in the extinction spectra corresponding to *y*- and *z*-polarized light, as would be expected, since the size and shape of the particle along its *y*- and *z*-axes are very similar. In contrast, the SPR excited by *x*-polarized light peaks at 399 nm and the value of the peak extinction efficiency is approximately 65% less than that of *z*-polarized light. Blue-shifting of the SPR for *x*-polarization compared to *y*- and *z*-polarizations is consistent with predictions of electromagnetic theory, since the *x*-axis corresponds to the truncated (short) axis of the particles. In this coordinate system, the experimental condition corresponds to an incident beam propagation direction along the *x*-axis. The *y*- and *z*-axes lie in the plane of the nanoparticle array and substrate. If one approximates the source lamp of the UV−vis spectrophotometer as a point source propagating solely in the *x*-direction, then the major components of the polarization vectors will lie in the *y*−*z* plane. Thus, in comparing theory to experiment, we will consider an average of *y*- and *z*-polarizations and omit *x*-polarization.

Figure 7 shows the calculated extinction spectrum of a single truncated tetrahedron for three different sets of values of the dielectric constant for bulk silver. The differences in the extinction spectra based on the choice of ϵ_{Ag} are very significant. The spectrum calculated using data from Johnson and Christy peaks at 550 nm, while that from Hagemann, Gudat, and Kunz peaks at 548 nm, versus the Palik value of 574 nm. We have chosen to use the dielectric constants from Palik because the values in the wavelength region of interest represent measurements obtained in an ultrahigh vacuum environment, which are therefore more reliable.

The calculated effect of particle−particle interaction between two truncated tetrahedra is shown in Figure 8. As the particles are brought closer together, the position of the SPR peak red-shifts. The results show that when the particles are separated by d_{tt} = 114 nm, which is the measured experimental separation, the interaction between two particles causes a red-shifting in the peak of the extinction spectrum of only about 5 nm, to 579 nm, compared to that of an isolated particle, whose peak is 574 nm. This implies that the nanoparticles in the array examined in this paper are influenced only to a small degree by their

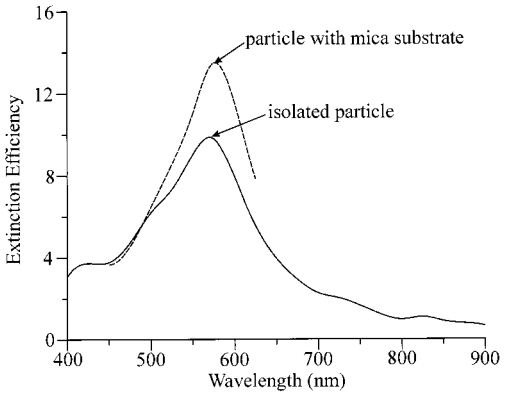

Figure 9. Effect of mica substrate ($\epsilon_{subs} = 2.55$) on the extinction spectrum of a single truncated tetrahedron. Results calculated using 2498 dipoles, dielectric constants from Palik, and polarization along the *y*-axis. Isolated particle: $\lambda_{max} = 570$ nm. Particle with mica substrate: $\lambda_{max} = 576$ nm.

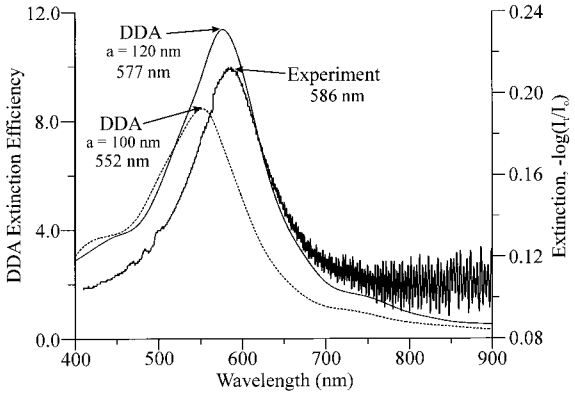

Figure 10. Comparison of measured UV−vis extinction of nanoparticle array on mica with "*a*" = 120 nm, "*b*" = 46 nm, and $d_{tt} = 114$ nm with calculated extinction of a single isolated truncated tetrahedron. Calculation 1 uses "*a*" = 120 nm, "*b*" = 46 nm, and 10 234 dipoles. Calculation 2 uses the tip-corrected value of "*a*" = 100 nm, "*b*" = 46 nm, and 10 548. Both results are calculated using ϵ_{Ag} of Palik and polarization averaged over *y*- and *z*-directions.

neighbors and for simplicity can be treated as though they were an array of individual, isolated particles. However, this is likely an underestimate of the interaction, since a given nanoparticle will interact with all three of its nearest neighbors and not just one.

The nanoparticles in the array are deposited on a mica substrate whose influence on the extinction spectrum must be examined. Figure 9 shows the extinction spectrum of a truncated tetrahedron with a mica substrate directly in contact with the base, compared with that of an isolated truncated tetrahedron. The dielectric function for mica used in this calculation was $\epsilon_{subs} = 2.55$.[44] Owing to the increased DDA calculation time when incorporating a substrate, the results presented here were calculated using 2498 dipoles and thus do not represent the fully converged result. The presence of the mica substrate red-shifts the SPR of the particle by only 6 nm. Considering that the effect of the substrate interaction on the SPR peak position is small and that the DDA calculation time is significantly increased when including particle−substrate interactions, it is a fair approximation to model the experimental particles on a mica substrate as isolated particles.

The comparison between the measured UV−vis extinction spectrum and the calculated extinction spectrum for a single isolated truncated tetrahedron is shown in Figure 10. We have provided the theoretical calculations for two different truncated tetrahedra: one using the particle width directly measured with the AFM, "*a*" = 120 nm, and one with a width that has been corrected for tip-broadening effects, "*a*" = 100 nm. In correcting for tip-broadening effects, we have assumed the ideal truncated tetrahedron cross-sectional line scan depicted in Figure 3B and a conical AFM tip with a radius of curvature of 10 nm and a 20° cone angle. Both calculations are averaged over *y* and *z* incident polarization directions and use slightly greater than 10 000 dipoles. The calculated surface plasmon resonance for the nanoparticle as measured and the tip-corrected nanoparticle peak at 577 and 552 nm, respectively, while the measured extinction maximum is 586 nm. The line shape of the calculated spectra closely matches that of the measured spectrum, with similar peak widths.

The fwhm peak width of the measured surface plasmon resonance spectrum is approximately 100 nm, or 0.35 eV. If one assumes that the nanoparticle array studied here is a purely homogeneous ensemble, then the peak width, Γ, corresponds to the lifetime of the electron−hole pair, τ, where $\tau = \hbar\Gamma^{-1}$. On the basis of the measured peak width, this lifetime is calculated to be 2 fs. The electron−hole pair lifetime is primarily determined by coupling between excited electrons and phonons in the metal, electron−electron interactions, and inhomogeneities of the system. A recent direct measurement of τ for a periodic array of particles fabricated by electron-beam lithography was 10 fs,[45] which is comparable to our indirect measurement.

It should be noted that the lithographically produced particle array is not perfect over the ~8 mm^2 area probed by the spectrophotometer. There are defects that occur as a result of imperfect packing of the polystyrene nanospheres. These defects are similar to those present in any crystal and include slip dislocations, missing nanoparticles, and multilayer packing. Slip dislocations are quite common and will result in the formation of long, narrow ridges of silver that separate domains of perfect packing (see Figure 1A). These are commonly 150 nm wide and 5−10 μm long. On the basis of our experiences in modeling various shapes of nanoparticles, we contend that the plasmon resonances of these highly prolate structures extend far into the infrared region of the spectrum and will therefore not influence the extinction measurements of the nanoparticle arrays in the 400−900 nm range. The number density of other smaller defects, such as single missing nanospheres, appears small enough to be insignificant.

We have recently acquired the ability to perform spatially resolved extinction spectroscopy at a resolution of 10−15 μm, which corresponds to the field of view of the AFM image shown in Figure 1A. Preliminary results show that the extinction spectra measured from different well-packed nanoparticle array areas such as that shown in Figure 1A are nearly identical to each other and to the macroscopic extinction result presented here. This supports the contention that the presence of defects plays a negligible role in the macroscopic, far-field UV−vis extinction spectrum.

Figure 11 shows the results of a DDA calculation that illustrate the individual contributions of absorption and scattering to the extinction spectrum for the "*a*" = 120 nm case from Figure 10. At the wavelength of peak extinction, 577 nm, the absorption comprises about 65% of the total extinction and scattering about 35%. The absorption peaks slightly blue of the extinction, at 574 nm, while the scattering peaks slightly red of the extinction, at 579 nm.

We can qualitatively correlate the measured extinction with the calculated extinction efficiency by making a few assumptions. The magnitude of the measured extinction at the peak

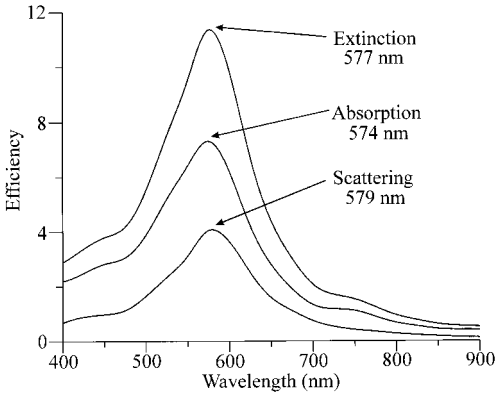

Figure 11. Relative contributions of scattering and absorption to calculated extinction spectrum for "*a*" = 120 nm and "*b*" = 46 nm truncated tetrahedron shown in Figure 10.

wavelength, E_{max}, is 0.11 extinction units. Assuming first that the area probed by the UV−vis spectrometer consists entirely of a perfectly packed nanoparticle array, the surface number density of particles, N, is 1.5×10^9 particles/cm^2. The extinction per particle, σ, ($\sigma = E_{max}/N$) is 7.3×10^{-11} cm^2/particle. The cross-sectional area, A, of a sphere having the same volume as the particle is 4.8×10^{-11} cm^2. Therefore, the extinction efficiency per particle, σ/A, is 1.5. However, a more realistic estimate of the actual percentage of the probed area covered with particles is 10−50%. Modifying the calculation to account for this more realistic coverage, we obtain an estimate for the magnitude of the extinction efficiency per particle between 3 and 15. Qualitatively, this is what we would expect, since the DDA calculates the peak extinction efficiency to be 11.4. The molar extinction coefficient, ϵ, assuming a 20% nanoparticle array surface coverage, is 2×10^{14} M^{-1} cm^{-1}, based on moles of silver nanoparticles, and 2×10^7 M^{-1} cm^{-1}, based on moles of silver atoms. This represents a very large extinction coefficient compared to a typical value on the order of 10^4−10^6 M^{-1} cm^{-1} for molecules with strong UV−vis absorption in solution.

V. Conclusions

The results show that the DDA can be used to quantitatively model the extinction spectra of nanofabricated silver particles. The position of the plasmon measured experimentally and the peak calculated using the tip-corrected measurement match within 34 nm. Including an estimate for the effects of substrate−particle and particle−particle interactions will red-shift the calculated peak by at least 10 nm and narrow the gap between the calculated and measured peaks. The remaining difference of about 25 nm between the calculated peak position for the tip-corrected particle and the measured peak extinction may be partly due to shortcomings of the truncated tetrahedron geometry in describing the actual shape of the particles. As we have seen from AFM images, the particle has rounded corners that are modeled as sharp edges with the truncated tetrahedron geometry. It is interesting to note that the total variation between the calculated surface plasmon resonances using different literature values for the bulk dielectric constants of silver is also about 25 nm. This implies that a large part of the 25 nm discrepancy between theory and experiment may arise from errors in the literature values of the bulk dielectric constants.

There are no adjustable parameters in the fitting of experiment to theory, since the structural information input to the calculation is obtained directly from AFM measurements. This work represents the first example of using electrodynamic theory to model the surface plasmon resonance spectrum of nonspheroidal metal nanoparticles with no adjustable parameters. A good match between experiment and theory has been achieved because of the structural homogeneity of the silver nanoparticles and the high level of electrodynamic theory employed.

It is likely that one will be able to use these results in order to design nanoparticle-based materials that are custom-tailored to provide high sensitivity in surface-enhanced Raman and related spectroscopies at user-selected excitation wavelengths. Furthermore, such nanoengineered materials may provide new strategies for optical modulation, optical limiting, and biosensing applications.

Acknowledgment. This research was supported by ARO Grant DAAG55-97-1-0133, PRF Grant 29507-AC6,5, National Science Foundation Grant CHE-940078, and the MRSEC program of the National Science Foundation Grant DMR-9632472.

References and Notes

(1) Oldenburg, S. J.; Averitt, R. D.; Westcott, S. L.; Halas, N. J. *Chem. Phys. Lett.* **1998**, *288*, 243−247.
(2) Emory, S. R.; Haskins, W. E.; Nie, S. *J. Am. Chem. Soc.* **1998**, *120*, 8009−8010.
(3) Fang, Y. *J. Chem. Phys.* **1998**, *108*, 4315−4318.
(4) Schaaff, T. G.; Shafigullin, M. N.; Khoury, J. T.; Vezmar, I.; Whetten, R. L.; Cullen, W. G.; First, P. N.; Gutérrez-Wing, C.; Ascensio, J.; Jose-Yacamán, M. J. *J. Phys. Chem. B* **1997**, *101*, 7885−7891.
(5) Feldstein, M. J.; Keating, C. D.; Liau, Y.-H.; Natan, M. J.; Scherer, N. F. *J. Am. Chem. Soc.* **1997**, *119*, 6638−6647.
(6) Logunov, S. L.; Ahmadi, T. S.; El-Sayed, M. A.; Khoury, J. T.; Whetten, R. L. *J. Phys. Chem. B* **1997**, *101*, 3713−3719.
(7) Lee, M. H.; Dobson, P. J.; Cantor, B. *Thin Solid Films* **1992**, *219*, 199−205.
(8) Roark, S. E.; Rowlen, K. L. *Anal. Chem.* **1994**, *66*, 261−270.
(9) Royer, P.; Bijeon, J. L.; Goudonnet, J. P.; Inagaki, R.; Arakawa, E. T. *Surf. Sci.* **1989**, *217*, 384−402.
(10) Creighton, J. A.; Eadon, D. G. *J. Chem. Soc., Faraday Trans.* **1991**, *87*, 3881−3891.
(11) Mulvaney, P. *Langmuir* **1996**, *12*, 788−800.
(12) van der Zande, B. M. I.; Böhmer, M. R.; Fokkink, L. G. J.; Schönenberger, C. *J. Phys. Chem. B* **1997**, *101*, 852−854.
(13) Yu, Y.-Y.; Chang, S.-S.; Lee, C.-L.; Wang, C. R. C. *J. Phys. Chem. B* **1997**, *101*, 6661−6664.
(14) Alvarez, M. M.; Khoury, J. T.; Schaaff, T. G.; Shafigullin, M. N.; Vezmar, I.; Whetten, R. L. *J. Phys. Chem. B* **1997**, *101*, 3706−3712.
(15) Taleb, A.; Petit, C.; Pileni, M. P. *J. Phys. Chem. B* **1998**, *102*, 2214−2220.
(16) Lisiecki, I.; Billoudet, F.; Pileni, M. P. *J. Phys. Chem.* **1996**, *100*, 4160−4166.
(17) Chernov, S. F.; Zakharov, V. N. *J. Mod. Opt.* **1989**, *36*, 1541−1544.
(18) Craighead, H. G.; Niklasson, G. A. *Appl. Phys. Lett.* **1984**, *44*, 1134−1136.
(19) Buncick, M. C.; Warmack, R. J.; Ferrell, T. L. *J. Opt. Soc. Am. B* **1987**, *4*, 927−933.
(20) Foss, C. A., Jr.; Tierney, M. J.; Martin, C. R. *J. Phys. Chem.* **1992**, *96*, 9001−9007.
(21) Gotschy, W.; Vonmetz, K.; Leitner, A.; Aussenegg, F. R. *Opt. Lett.* **1996**, *21*, 1099−1101.
(22) Kreibig, U. Optics of Nanosized Metals. In *Handbook of Optical Properties. Optics of Small Particles, Interfaces, and Surfaces*; Hummel, R. E., Wissmann, P., Eds.; CRC Press: Boca Raton, FL, 1997; Vol. II., pp 145−190.
(23) Papavassiliou, G. C. *Prog. Solid State Chem.* **1980**, *12*, 185−271.
(24) Bohren, C. F.; Huffman, D. R. *Absorption and Scattering of Light by Small Particles*; John Wiley & Sons: New York, 1983.
(25) Mie, G. *Ann. Phys.* **1908**, *25*, 377.
(26) Klar, T.; Perner, M.; Grosse, S.; von Plessen, G.; Spirkl, W.; Feldmann, J. *Phys. Rev. Lett.* **1998**, *80*, 4249−4252.
(27) Hornyak, G. L.; Martin, C. R. *Thin Solid Films* **1997**, *303*, 84−88.
(28) Hornyak, G. L.; Patrissi, C. J.; Martin, C. R. *J. Phys. Chem. B* **1997**, *101*, 1548−1555.
(29) Barber, P. W.; Chang, R. K.; Massoudi, H. *Phys. Rev. B* **1983**, *27*, 7251−7261.
(30) Barber, P. W.; Chang, R. K.; Massoudi, H. *Phys. Rev. Lett.* **1983**, *50*, 997−1000.

(31) Al-Rawashdeh, N. A. F.; Sandrock, M. L.; Seugling, C. J.; Foss, C. A., Jr. *J. Phys. Chem. B* **1998**, *102*, 361−371.
(32) Hulteen, J. C.; Van Duyne, R. P. *J. Vac. Sci. Technol. A* **1995**, *13*, 1553−1558.
(33) Hulteen, J. C.; Treichel, D. A.; Van Duyne, R. P. *J. Phys. Chem. B*, submitted.
(34) Yang, W. H.; Schatz, G. C.; Van Duyne, R. P. *J. Chem. Phys.* **1995**, *103*, 869−875.
(35) Jensen, T.; Kelly, L.; Lazarides, A.; Schatz, G. C. *J. Cluster Sci*. **1998**, in press.
(36) Purcell, E. M.; Pennypacker, C. R. *Astrophys. J.* **1973**, *186*, 705−714.
(37) Draine, B. T.; Flatau, P. J. *J. Opt. Soc. Am. A* **1994**, *11*, 1491.
(38) Draine, B. T.; Goodman, J. *Astrophys. J.* **1993**, *405*, 685−697.
(39) Jensen, T. R.; Duval, M. L.; Schatz, G. C.; Van Duyne, R. P. Manuscript in preparation.
(40) Draine, B. T.; Flatau, P. J. *Program DDSCAT*, version 4b.1; University of California, San Diego, Scripps Institute of Oceanography: La Jolla, CA, 1993.
(41) Palik, E. D. *Handbook of Optical Constants of Solids*; Academic Press: New York, 1985.
(42) Hagemann, H.-J.; Gudat, W.; Kunz, C. *J. Opt. Soc. Am.* **1975**, *65*, 742−744.
(43) Johnson, P. B.; Christy, R. W. *Phys. Rev. B* **1972**, *6*, 4370−4379.
(44) Lide, D. R. *Handbook of Chemistry and Physics*, 71st ed.; CRC Press: Boca Raton, FL, 1990.
(45) Lamprecht, B.; Leitner, A.; Aussenegg, F. R. *Appl. Phys. B* **1997**, *64*, 269−272.